

Primordial black holes from the perturbations in the inflaton potential in peak theory

Qing Wang^a Yi-Chen Liu^a Bing-Yu Su^a and Nan Li^{a,1}

^a*Department of Physics, College of Sciences, Northeastern University
No. 3-11, Wenhua Road, Shenyang, 110819, China*

E-mail: linan@mail.neu.edu.cn

ABSTRACT: The primordial black hole (PBH) is an effective candidate for dark matter. In this work, the PBH abundance f is calculated in peak theory, with one or two perturbations in the inflaton potential. We construct an antisymmetric perturbation that can create a perfect plateau in the inflaton potential, leading inflation to the ultra-slow-roll stage. During this stage, the power spectrum of primordial curvature perturbation is remarkably enhanced on small scales, generating abundant PBHs. The PBH abundance $f \sim 0.1$ can be achieved in one or two typical mass windows at $10^{-17}M_{\odot}$, $10^{-13}M_{\odot}$, and $30M_{\odot}$, without spoiling the nearly scale-invariant power spectrum on large scales. For comparison, f is calculated in two approximate methods of peak theory (with different spectral moments) and also in the Press–Schechter theory. It is found that the Press–Schechter theory systematically underestimates f by two or three orders of magnitude compared with peak theory.

¹Corresponding author.

Contents

1	Introduction	1
2	PBH abundance	3
2.1	Basic equations	4
2.2	Power spectrum	5
2.3	PBH mass and abundance	6
3	Peak theory and PS theory	7
3.1	Peak theory	7
3.2	High-peak approximation	8
3.3	GLMS approximation	9
3.4	PS theory	9
4	PBHs from one perturbation in the inflaton potential	10
5	PBHs from two perturbations in the inflaton potential	14
6	Comparison of peak and PS theories	17
7	Conclusion	19

1 Introduction

Primordial black holes (PBHs) have been receiving increasing research interest in recent years, especially after the discovery of the long-sought gravitational waves (GWs) from the merger of binary black holes [1]. The influences of PBHs in cosmology are manifold. For instance, the PBHs can be the sources of GWs [2], and their Hawking radiation can also change the background intensities of various cosmic rays [3]. Moreover, they can be utilized as a probe in the very early Universe to constrain the inflation models [4, 5]. Most importantly, the PBH is a natural candidate for dark matter (DM) (e.g., as the seeds of super-massive black holes in the centers of galaxies) [6, 7].

PBHs can be formed in many different ways in the radiation-dominated era of the early Universe, such as various phase transitions [3, 5, 7]. Nevertheless, the simplest picture is the direct collapse of the radiation field, when its density fluctuation exceeds some certain threshold [8–11]. Different from astrophysical black holes, PBHs have a vast mass range spanning over 40 orders of magnitude, from the Planck mass to super-massive scale ($10^{-5} \sim 10^{40}$ g), without the lower bound around $3M_{\odot}$ or the mass gap around $50 \sim 120M_{\odot}$ ($M_{\odot} = 1.989 \times 10^{33}$ g denotes the solar mass). Because of the Hawking radiation, PBHs

with $M < 10^{15}$ g have already evaporated, and PBHs with $M > 10^{15}$ g can still exist today, acting as a stable and pressureless candidate for DM.

The PBH abundance f is defined as its proportion in the DM density at present, and the experimental constraints on PBHs refer to the upper bounds of f in different mass ranges. If $f \sim 0.1$, PBHs can be considered as an effective candidate for DM; if $f \ll 10^{-3}$, its possibility as DM can be safely excluded from the relevant mass range. According to various constraints from the evaporation, lensing, dynamics, accretion, and GW experiments, there still remain three open mass windows: the asteroid mass range ($10^{-17} \sim 10^{-16} M_\odot$), the sub-lunar mass range ($10^{-13} \sim 10^{-9} M_\odot$), and the intermediate mass range ($10 \sim 10^3 M_\odot$) [7]. (For more recent and complete constraints on the PBHs, see [12].)

Generally speaking, in order to achieve the PBH abundance $f \sim 0.1$, the radiation field must possess a sufficiently large density fluctuation, with the power spectrum of primordial curvature perturbation $\mathcal{P}_\mathcal{R}$ enhanced up to at least 10^{-2} on small scales. However, such a large magnitude cannot be obtained in the usual single-field slow-roll (SR) inflation models, which generate a nearly scale-invariant power spectrum only on large scales [e.g., $\mathcal{P}_\mathcal{R}$ is just around 10^{-9} on the pivot scale k_* of the cosmic microwave background (CMB) [13]]. Consequently, the SR conditions should be violated on small scales, and this violation can be realized by the so-called ultra-slow-roll (USR) stage in the inflationary era [14–68].

If there is a plateau or a saddle point in the single- or multi-field inflaton potential V , the inflaton will roll down its potential extremely slowly, resulting in a remarkable enhancement of $\mathcal{P}_\mathcal{R}$ and a considerable PBH abundance simultaneously. The USR conditions can be realized in many ways. For example, one may consider the (near-)inflection points in V , but the specific form of V must be designed very carefully, so that the USR inflation increases $\mathcal{P}_\mathcal{R}$ only on small scales but does not spoil the CMB physics on large scales. Instead, in this paper, we take another approach and investigate the USR inflation and the PBH abundance by imposing one or two perturbations δV on the background potential V . By this means, the USR inflation can be studied on small and large scales separately, without the troublesome interference in between [29, 49, 54, 62, 63]. The essential difference between our work and the previous literature is a new construction of the perturbations. Usually, these perturbations were chosen to be symmetric (e.g., Gaussian) in the USR region, but V itself must not be symmetric there—otherwise, the inflaton cannot roll down at all. Therefore, we now choose an antisymmetric perturbation that can be imposed on V more smoothly on both sides of the USR region. As a result, there can be a plateau flat enough in V , and the USR stage can be maintained for a sufficiently long time, generating the PBHs with desirable masses and abundances.

In this paper, we numerically calculate the power spectrum $\mathcal{P}_\mathcal{R}$ and the PBH abundance f in the single-field inflation models, with one or two perturbations in the inflaton potential, as the analytical SR approximations can no longer be trusted in the USR stage. We demand the PBH abundance $f \sim 0.1$ in one or two typical mass windows at $10^{-17} M_\odot$, $10^{-13} M_\odot$, and $30 M_\odot$. Here, we should mention that f is affected by many factors, such as the choice of window function, the threshold of density contrast, and the method to calculate the PBH mass fraction. Below, we focus on the last aspect, calculate the PBH mass fraction and abundance in peak theory [69–79], and compare the results with those obtained from the

Press–Schechter (PS) theory [80].

The peak theory of Gaussian random fields was initiated in Ref. [70]. Furthermore, in Ref. [71], Green, Liddle, Malik, and Sasaki (GLMS) calculated the PBH abundance via a simplified peak theory and arrived at the results in reasonable agreement with the PS theory, but only for the power spectrum in the power-law form. Their results were later extended to the scale-invariant power spectrum and the power spectrum with a running spectral index [72], and the PBH abundances obtained from peak and PS theories were found to be different but still similar, within a factor of $\mathcal{O}(10)$. The peak theory with local non-Gaussianity was discussed in Ref. [74], the point-peak approximation was presented in Ref. [77], and the optimized peak theory was also explored in Ref. [79]. In general, the PBH abundances obtained in various peak theories are always larger than that from the PS theory, but the detailed ratio depends on the specific profile of density fluctuations [73, 78].

The basic idea of peak theory is to calculate the number density of peaks where compact objects like galaxies and PBHs are expected to form, if the density contrast δ exceeds some threshold δ_c . As the peaks correspond to the local maxima of δ , peak theory deals with a multi-dimensional joint probability distribution function (PDF) of δ and its first- and second-order spatial derivatives. In order to obtain the one-dimensional conditional PDF of δ , we must perform the dimensional reduction on the multi-dimensional PDF by a series of integrations. The general peak theory is very complicated, and the approximations at different levels have been developed for various practical aims, especially for the large density contrast in the PBH formation. In these approximations, we are confronted with the spectral moments σ_i of density contrast at different orders. In Sec. 3, we refer the high-peak approximation to the one including σ_0 , σ_1 , and σ_2 and the GLMS approximation to the one including σ_0 and σ_1 . As a comparison, the simplest PS theory involves only σ_0 and can be viewed as the limit case of the general peak theory. All these three cases will be discussed and compared in detail below.

This paper is organized as follows. In Sec. 2, we study the power spectrum and calculate the PBH mass and abundance. In Sec. 3, we review the general peak theory and the relevant high-peak and GLMS approximations. The PS theory is also discussed for comparison. Then, in Sects. 4 and 5, we study the power spectra and PBH abundances in the GLMS approximation, with one or two perturbations in the inflaton potential, respectively. Finally, a general comparison of the PBH abundances in peak and PS theories is presented in Sec. 6. We conclude in Sec. 7. We work in the natural system of units and set $c = \hbar = k_B = 1$.

2 PBH abundance

In this section, we discuss the power spectrum of primordial curvature perturbation, explain the significant difference between the SR and USR inflations, and calculate the PBH mass and abundance in detail.

2.1 Basic equations

We start from the single-field inflation model, in which inflation is supported by a scalar inflaton field minimally coupled to gravity, with the action reading

$$S = \int d^4x \sqrt{-g} \left[\frac{m_{\text{P}}^2}{2} R - \frac{1}{2} \partial_\mu \phi \partial^\mu \phi - V(\phi) \right],$$

where ϕ is the inflaton field, $V(\phi)$ is its potential, R is the Ricci scalar, and $m_{\text{P}} = 1/\sqrt{8\pi G}$ is the Planck mass. In the inflationary era, it is more convenient to measure the cosmic expansion in terms of the number of e -folds N instead of the cosmic time t , which is defined as $dN = H(t) dt = d \ln a$. Here, $a = e^N$ is the scale factor, and $H = \dot{a}/a$ is the Hubble expansion rate. In order to solve the flatness and horizon problems in the standard Big Bang cosmology, the Universe must experience a quasi-de Sitter expansion, with N being around 70.

Two useful parameters can be introduced to characterize the motion of the inflaton field,

$$\varepsilon = -\frac{\dot{H}}{H^2}, \quad \eta = -\frac{\ddot{\phi}}{H\dot{\phi}}.$$

Usually, they are named as the SR parameters, as in the SR inflation, ε and $|\eta|$ are both much smaller than 1. However, they can also be applied to other circumstances like the USR stage, during which they change drastically, and this is of essential importance in calculating the PBH abundance.

In terms of ε , η , and N , in the homogeneous and isotropic Universe, the Klein–Gordon equation for the inflaton field ϕ is

$$\phi_{,NN} + (3 - \varepsilon)\phi_{,N} + \frac{1}{H^2} V_{,\phi} = 0, \quad (2.1)$$

and the Friedmann equation for the cosmic expansion is

$$H^2 = \frac{V}{(3 - \varepsilon)m_{\text{P}}^2}. \quad (2.2)$$

Furthermore, we study the perturbations on the background space-time, with the perturbed metric reading $ds^2 = -(1 + 2\Phi) dt^2 + a^2(t)(1 - 2\Phi)\delta_{ij} dx^i dx^j$. Here, we neglect the anisotropic stress and focus only on the scalar perturbation Φ , as the vector and tensor perturbations are irrelevant to the production of PBHs. A more useful gauge-invariant scalar perturbation is the primordial curvature perturbation \mathcal{R} , which can be used to calculate the PBH abundance,

$$\mathcal{R} = \Phi + \frac{H}{\dot{\phi}} \delta\phi.$$

The equation of motion for \mathcal{R} in the Fourier space is the Mukhanov–Sasaki equation,

$$\mathcal{R}_{k,NN} + (3 + \varepsilon - 2\eta)\mathcal{R}_{k,N} + \frac{k^2}{H^2 e^{2N}} \mathcal{R}_k = 0. \quad (2.3)$$

Moreover, ε and η can also be expressed in terms of N ,

$$\varepsilon = \frac{\phi_{,N}^2}{2m_{\text{P}}^2}, \quad \eta = \frac{\phi_{,N}^2}{2m_{\text{P}}^2} - \frac{\phi_{,NN}}{\phi_{,N}}. \quad (2.4)$$

Altogether, we will numerically solve Eqs. (2.1)–(2.4) to calculate the power spectrum and the PBH abundance in the following sections.

2.2 Power spectrum

The statistical properties of Gaussian random fields are completely encoded in the two-point correlation function (i.e., the power spectrum in the Fourier space). The PBH abundance can be calculated via the dimensionless power spectrum of primordial density contrast $\mathcal{P}_\delta(k)$. In the radiation-dominated era, $\mathcal{P}_\delta(k)$ can be further related to the dimensionless power spectrum of primordial curvature perturbation $\mathcal{P}_{\mathcal{R}}(k)$ [71],

$$\mathcal{P}_\delta(k) = \frac{16}{81} \left(\frac{k}{aH} \right)^4 \mathcal{P}_{\mathcal{R}}(k),$$

where

$$\mathcal{P}_{\mathcal{R}}(k) = \frac{k^3}{2\pi^2} |\mathcal{R}_k|^2 \Big|_{k \ll aH}.$$

In the SR inflation, $\mathcal{P}_{\mathcal{R}}(k)$ is nearly scale invariant,

$$\mathcal{P}_{\mathcal{R}}(k) = \frac{1}{8\pi^2\varepsilon} \left(\frac{H}{m_{\text{P}}} \right)^2, \quad (2.5)$$

and can be usually written in the power-law form as $\mathcal{P}_{\mathcal{R}}(k) = A_{\text{s}}(k/k_*)^{n_{\text{s}}-1}$, where n_{s} is the scalar spectral index and A_{s} is the amplitude, with the central values being $n_{\text{s}} = 0.965$ and $A_{\text{s}} = 2.10 \times 10^{-9}$ on the CMB pivot scale $k_* = 0.05 \text{ Mpc}^{-1}$ [13]. However, on small scales where PBHs are expected, the constraints on $\mathcal{P}_{\mathcal{R}}(k)$ are still rather loose [3, 5, 7] (the CMB observations cover only about 10 e -folds on large scales). In particular, in the USR region, both numerical and analytical investigations indicate $n_{\text{s}} - 1 \approx 4$ in the growing stage of $\mathcal{P}_{\mathcal{R}}(k)$ [39, 47].

Now, we first need to smooth the density contrast δ on a large scale, usually taken as $R = 1/(aH)$, in order to avoid the non-differentiability and the divergence in the large- k limit of the radiation field. This smoothing procedure can be realized by a convolution of δ as $\delta(\mathbf{x}, R) = \int d^3x' W(\mathbf{x} - \mathbf{x}', R)\delta(\mathbf{x}')$, with $W(\mathbf{x}, R)$ being the window function. Below, we choose Gaussian window function, with its Fourier transform being $\widetilde{W}(k, R) = e^{-k^2 R^2/2}$. Hence, the window function in real space is $W(\mathbf{x}, R) = e^{-x^2/(2R^2)}/V(R)$, and the volume $V(R) = (\sqrt{2\pi}R)^3$ is the normalization factor.

The variance of the smoothed density contrast on the scale R can be calculated as

$$\sigma_\delta^2(R) = \langle \delta^2(\mathbf{x}, R) \rangle = \int_0^\infty \frac{dk}{k} \widetilde{W}^2(k, R) \mathcal{P}_\delta(k),$$

where $\langle \dots \rangle$ denotes the ensemble average, and we have used the fact $\langle \delta(\mathbf{x}, R) \rangle = 0$ for a Gaussian random field. Moreover, the homogeneity and isotropy of the background Universe guarantees that $\sigma_\delta^2(R)$ is independent of a special position \mathbf{x} . Similarly, the i -th spectral moment of the smoothed density contrast is defined as

$$\sigma_i^2(R) = \int_0^\infty \frac{dk}{k} k^{2i} \widetilde{W}^2(k, R) \mathcal{P}_\delta(k) = \frac{16}{81} \int_0^\infty \frac{dk}{k} k^{2i} \widetilde{W}^2(k, R) (kR)^4 \mathcal{P}_\mathcal{R}(k),$$

where $i = 0, 1, 2, \dots$, and $\sigma_0 = \sigma_\delta$ naturally.

For the convenience of expression in Sec. 3, two new important factors in peak theory are introduced here. The first one is the relative density contrast,

$$\nu = \frac{\delta}{\sigma_\delta},$$

and its corresponding threshold is $\nu_c = \delta_c / \sigma_\delta$. The specific value of δ_c depends on the equation of state of the cosmic medium and many other ingredients [81–91] and is the most influential factor in calculating the PBH abundance. In this paper, we follow Ref. [85] and set $\delta_c = 0.414$. In Sec. 6, it will be shown that ν_c should be around $\mathcal{O}(10)$, so as to achieve abundant PBHs, and ν_c is not a constant, as σ_δ depends on the smoothing scale R . Furthermore, the second factor is defined as

$$\gamma = \frac{\sigma_1^2}{\sigma_\delta \sigma_2}.$$

The γ factor encodes the specific information of the profile of density contrast, and it is easy to find $0 < \gamma < 1$ by definition. Also, in Sec. 6, it will be shown that $\gamma \approx 1$ for the PBH formation.

2.3 PBH mass and abundance

In the Carr–Hawking collapse model [10], the PBH mass M can be related to the horizon mass at the time of its formation,

$$M = \kappa M_{\text{H}} = \frac{\kappa}{2GH},$$

where $M_{\text{H}} = 1/(2GH)$ is the horizon mass, and κ is the efficiency of collapse. In the radiation-dominated era, $H = 1/(2t)$, so $M = \kappa t/G$. From the conservation of entropy in the adiabatic cosmic expansion, we have [3]

$$\frac{M}{M_\odot} = 1.13 \times 10^{15} \left(\frac{\kappa}{0.2} \right) \left(\frac{g_*}{106.75} \right)^{-1/6} \left(\frac{k_*}{k_{\text{PBH}}} \right)^2, \quad (2.6)$$

where g_* is the effective number of relativistic degrees of freedom of energy density, and $k_{\text{PBH}} = 1/R$ is the wave number of the PBH that exits the horizon. Below, we follow Ref. [11] and choose $\kappa = 0.2$ and $g_* = 106.75$. From Eq. (2.6), all spectral moments $\sigma_i(R)$ can be reexpressed in terms of the PBH mass as $\sigma_i(M)$.

Furthermore, the PBH mass fraction $\beta(M)$ at the time of its formation is defined as

$$\beta(M) = \left. \frac{\rho_{\text{PBH}}(M)}{\rho_{\text{R}}} \right|_{\text{formation}}.$$

For the massive PBHs not evaporated yet (ignoring their radiation, accretion, and merger), their abundance at present is defined as

$$f(M) = \left. \frac{\rho_{\text{PBH}}(M)}{\rho_{\text{DM}}} \right|_{\text{today}}.$$

Naturally, $f(M)$ is proportional to $\beta(M)$ [3],

$$f(M) = 1.68 \times 10^8 \left(\frac{M}{M_{\odot}} \right)^{-1/2} \beta(M). \quad (2.7)$$

Here, we should stress that the PBH mass M has the same expression in peak and PS theories, but the PBH mass fraction β and abundance f are different in various peak theories and the PS theory. All these issues will be systematically investigated in this paper.

3 Peak theory and PS theory

In this section, we briefly review the peak theory of Gaussian random fields and present the general formula for the PBH mass fraction β . For comparison, the simplified results of β are shown in the high-peak approximation, the GLMS approximation, and the PS theory, respectively.

3.1 Peak theory

The general peak theory of Gaussian random fields in Ref. [70] can also be applied to calculate the PBH abundance, with the peak value being the relative density contrast ν . The number density of peaks is $n(\mathbf{r}) = \sum_p \delta_{\text{D}}(\mathbf{r} - \mathbf{r}_p)$, where δ_{D} is the three-dimensional Dirac function, and \mathbf{r}_p is the position where δ has a local maximum. This maximum condition further demands that the first-order derivative $\partial_i \delta$ vanishes ($i = 1, 2, 3$) and the second-order derivative $\partial_i \partial_j \delta$ is negative definite at \mathbf{r}_p ($i, j = 1, 2, 3$). Since δ is assumed to be Gaussian, $\partial_i \delta$ and $\partial_i \partial_j \delta$ are also Gaussian accordingly. Altogether, we should deal with the ten-dimensional joint PDF $P(\{y_i\})$ of Gaussian variables (one for δ , three for $\partial_i \delta$, and six for $\partial_i \partial_j \delta$ due to its symmetry),

$$P(\{y_i\}) = \frac{1}{\sqrt{(2\pi)^{10} \det \mathcal{M}}} \exp \left(\frac{1}{2} \sum_{ij} \Delta y_i \mathcal{M}_{ij}^{-1} \Delta y_j \right),$$

where \mathcal{M} is the covariance matrix, and $\Delta y_i = y_i - \langle y_i \rangle$, with $y_1 = \delta$, $y_2 = \partial_1 \delta$, \dots , $y_5 = \partial_1 \partial_1 \delta$, \dots , and $y_{10} = \partial_2 \partial_3 \delta$.

From Ref. [70], a series of dimensional reductions can finally lead the ten-dimensional joint PDF $P(\{y_i\})$ to the one-dimensional conditional PDF $P(\nu)$. By means of $P(\nu)$, the

number density of peaks $n(\nu_c)$ with $\nu > \nu_c$ can be written in a more convenient integral form of the one-dimensional differential number density $\mathcal{N}(\nu)$,

$$n(\nu_c) = \int_{\nu_c}^{\infty} \mathcal{N}(\nu) d\nu = \frac{1}{(2\pi)^2 R_*^3} \int_{\nu_c}^{\infty} G(\gamma, \nu) e^{-\nu^2/2} d\nu,$$

where $R_* = \sqrt{3}\sigma_1/\sigma_2$, and

$$G(\gamma, \nu) = \int_0^{\infty} \frac{f(x)}{\sqrt{2\pi(1-\gamma^2)}} \exp\left[\frac{-(x-\gamma\nu)^2}{2(1-\gamma^2)}\right] dx, \quad (3.1)$$

with

$$f(x) = \frac{x^3 - 3x}{2} \left[\operatorname{erf}\left(\sqrt{\frac{5}{2}}x\right) + \operatorname{erf}\left(\sqrt{\frac{5}{8}}x\right) \right] + \sqrt{\frac{2}{5\pi}} \left[\left(\frac{31x^2}{4} + \frac{8}{5}\right) e^{-5x^2/8} + \left(\frac{x^2}{2} - \frac{8}{5}\right) e^{-5x^2/2} \right].$$

The constraint condition that the peak position corresponds to the local maximum of density contrast is encoded in the $G(\gamma, \nu)$ function implicitly.

Finally, the PBH mass fraction at the time of its formation can be obtained in peak theory as

$$\beta = n(\nu_c)V(R) = \frac{1}{\sqrt{2\pi}} \left(\frac{R}{R_*}\right)^3 \int_{\nu_c}^{\infty} G(\gamma, \nu) e^{-\nu^2/2} d\nu. \quad (3.2)$$

In general, there are the zeroth, first, and second spectral moments σ_δ , σ_1 , and σ_2 in β implicitly. Retaining these moments to different orders corresponds to different approximate peak theories and induces different formulae for β , to be explained explicitly below.

3.2 High-peak approximation

The high-peak approximation keeps all three spectral moments σ_δ , σ_1 , and σ_2 , and the approximation refers to the condition $\gamma\nu \gg 1$. As $0 < \gamma < 1$, we have $\nu \gg 1$ (i.e., $\delta \gg \sigma_\delta$). This can always be guaranteed, as the PBH formation is a rather rare event.

In the limit of $\gamma\nu \gg 1$, the part of the integrand in Eq. (3.1), $\frac{1}{\sqrt{2\pi(1-\gamma^2)}} \exp\left[\frac{-(x-\gamma\nu)^2}{2(1-\gamma^2)}\right]$, behaves as the Dirac function, so only the values around $x = \gamma\nu$ significantly contribute to the integral. When $x \gg 1$, the asymptotic expansion of $f(x)$ is $f(x) = x^3 - 3x$, so $G(\gamma, \nu) = (\gamma\nu)^3 - 3\gamma\nu$. Substituting $G(\gamma, \nu)$ into Eq. (3.2), we obtain the PBH mass fraction in the high-peak approximation,

$$\beta_{\text{hp}} = \frac{1}{\sqrt{2\pi}} Q^3 \left(\nu_c^2 + 2 - \frac{3}{\gamma^2} \right) e^{-\nu_c^2/2}, \quad (3.3)$$

where $Q = R\sigma_1/(\sqrt{3}\sigma_\delta)$.

3.3 GLMS approximation

A more frequently used peak theory is the GLMS approximation, which is a further step of the high-peak approximation. Besides the condition $\gamma\nu \gg 1$, it also demands $\gamma = \sigma_1^2/(\sigma_\delta\sigma_2) \approx 1$. This means that σ_2 is not independent of σ_δ and σ_1 , so only two spectral moments σ_δ and σ_1 are enough in the GLMS approximation.

In Refs. [70, 71], the $G(\gamma, \nu)$ function was obtained in the above approximations,

$$G(\gamma, \nu) = \left[\frac{\langle k^2(R) \rangle}{3} \right]^{3/2} R_*^3 (\nu^3 - 3\nu),$$

where $\langle k^2(R) \rangle$ is a function of the smoothing scale R ,

$$\langle k^2(R) \rangle = \frac{1}{\langle \delta^2(R) \rangle} \int_0^\infty \frac{dk}{k} k^2 \widetilde{W}^2(k, R) \mathcal{P}_\delta(k) = \frac{\sigma_1^2}{\sigma_\delta^2}.$$

Hence, we obtain $G(\nu) = \nu^3 - 3\nu$, so the $G(\gamma, \nu)$ function depends only on ν in the GLMS approximation. Substituting $G(\nu)$ into Eq. (3.2), we obtain the PBH mass fraction in the GLMS approximation,

$$\beta_{\text{GLMS}} = \frac{1}{\sqrt{2\pi}} Q^3 (\nu_c^2 - 1) e^{-\nu_c^2/2}. \quad (3.4)$$

It is straightforward to find that Eq. (3.3) is reduced to Eq. (3.4) when $\gamma \approx 1$.

3.4 PS theory

In the PS theory, the $G(\gamma, \nu)$ function is simply taken as a constant, $G = (R_*/R)^3$, independent of γ or ν , so from Eq. (3.2), the PS theory involves only the zeroth spectral moment σ_0 (i.e., the variance of density contrast σ_δ). Therefore, it is a non-physical dimensional reduction of the general peak theory and can be regarded as its limit case.

Substituting G into Eq. (3.2), it is easy to find that the PS theory is equivalent to directly assuming the PDF $P(\nu)$ to be Gaussian, $P(\nu) = e^{-\nu^2/2}/\sqrt{2\pi}$. Considering $\nu_c \gg 1$, we obtain the PBH mass fraction in the PS theory,

$$\beta_{\text{PS}} = \frac{1}{2} \text{erfc} \left(\frac{\nu_c}{\sqrt{2}} \right) \approx \frac{1}{\sqrt{2\pi}\nu_c} e^{-\nu_c^2/2}. \quad (3.5)$$

Summarizing and comparing the results in Eqs. (3.3)–(3.5), we find that β_{GLMS} is the largest PBH mass fraction but is only slightly larger than β_{hp} . Moreover, at the leading order of ν_c , we obtain

$$\frac{\beta_{\text{PS}}}{\beta_{\text{hp}}} \approx \frac{\beta_{\text{PS}}}{\beta_{\text{GLMS}}} \approx \frac{1}{(Q\nu_c)^3}. \quad (3.6)$$

In Sec. 6, it will be shown that the values of $1/(Q\nu_c)^3$ can be as small as $10^{-3} \sim 10^{-2}$. Consequently, there is a systematic bias between the PS theory and the high-peak or GLMS approximation, and the PS theory leads to a significant underestimation of the PBH abundance.

4 PBHs from one perturbation in the inflaton potential

From the discussions in Secs. 2 and 3, the procedure to calculate the PBH abundance can be summarized as

$$\delta V(\phi) \rightarrow \mathcal{P}_{\mathcal{R}}(k) \rightarrow \sigma_i^2(M) \rightarrow \beta(M) \rightarrow f(M).$$

The discrepancy among the high-peak approximation, the GLMS approximation, and the PS theory lies in the intermediate steps $\mathcal{P}_{\mathcal{R}}(k) \rightarrow \sigma_i^2(M) \rightarrow \beta(M)$, and the first and last steps $\delta V(\phi) \rightarrow \mathcal{P}_{\mathcal{R}}(k)$ and $\beta(M) \rightarrow f(M)$ are the same under all circumstances. In this section, we first construct a suitable form for one perturbation $\delta V(\phi)$ in the inflaton potential and then achieve the PBH abundance $f \sim 0.1$ in the GLMS approximation in the three typical mass windows at $10^{-17}M_{\odot}$, $10^{-13}M_{\odot}$, and $30M_{\odot}$, respectively (the PBH abundances in the high-peak approximation and the PS theory will be discussed in Sec. 6). The difference between the power spectra $\mathcal{P}_{\mathcal{R}}(k)$ in the SR and USR inflations will also be illustrated.

In general, the specific form of the perturbation $\delta V(\phi)$ is not unique, as long as it can smooth the background inflaton potential $V_b(\phi)$ at some position ϕ_0 . In this way, a plateau appears around ϕ_0 , leading inflation to the USR stage and thus enhancing the power spectrum and the PBH abundance. Previously, some attempts (e.g., Gaussian perturbation) were considered in Refs. [29, 49, 54, 62, 63]. Gaussian $\delta V(\phi)$ is symmetric in the USR region, but $V_b(\phi)$ itself cannot be symmetric and must have a certain slope, if the inflaton can roll down there. Hence, $\delta V(\phi)$ and $V_b(\phi)$ cannot be connected very smoothly on both sides of ϕ_0 . As a result, the inflaton either still rolls down $V_b(\phi)$ rapidly after the USR stage or even cannot surmount the perturbation and stops in the USR region, resulting in eternal inflation.

Therefore, in this paper, we suggest a new antisymmetric form of the perturbation as

$$\delta V(\phi) = -A(\phi - \phi_0)F\left(\frac{\phi - \phi_0}{\sqrt{2}\sigma}\right), \quad (4.1)$$

where F is an even function for the argument and satisfies $\lim_{x \rightarrow \infty} xF(x) = 0$. There are three parameters in our model: A , ϕ_0 , and σ , characterizing the slope, position, and width of $\delta V(\phi)$, respectively. Thus, if A is very close to $V_{b,\phi}(\phi_0)$, a perfect plateau can be created around ϕ_0 . In this way, the inflaton can pass the perturbation definitely, and the USR stage can be maintained for a sufficiently long time, generating abundant PBHs. In Secs. 4 and 5, we will choose F to be Lorentzian and Gaussian functions, in order to verify the applicability and universality of our model.

Below, the background inflaton potential $V_b(\phi)$ is taken as the Kachru–Kallosh–Linde–Trivedi potential [92],

$$V_b(\phi) = V_0 \frac{\phi^2}{\phi^2 + (m_{\text{P}}/2)^2}, \quad (4.2)$$

where we set $V_0/m_{\text{P}}^4 = 10^{-10}$, so there can be a nearly scale-invariant power spectrum $\mathcal{P}_{\mathcal{R}}(k)$ on large scales and a relatively small tensor-to-scalar ratio r favored by the CMB

observations [13]. Furthermore, F is chosen to be Lorentzian function, so the perturbation $\delta V(\phi)$ is

$$\delta V(\phi) = -A \frac{(\phi - \phi_0)}{1 + (\phi - \phi_0)^2 / (2\sigma^2)}. \quad (4.3)$$

Altogether, the inflaton potential reads $V(\phi) = V_b(\phi) + \delta V(\phi)$, as plotted in Fig. 1.

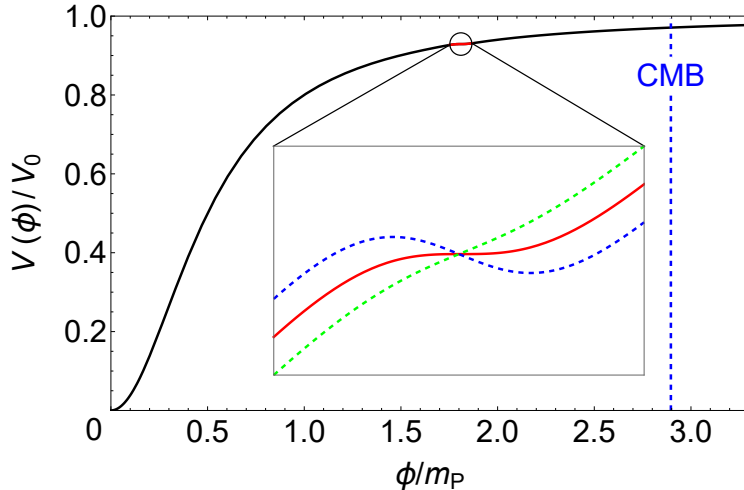


Figure 1. The background inflaton potential $V_b(\phi)$ in Eq. (4.2) and the plateau (i.e., the USR region) caused by the perturbation $\delta V(\phi)$ in Eq. (4.3), with $\phi_0/m_P = 1.81$ and $\sigma/m_P = 0.057$. For comparison, A is chosen to be $0.5V_{b,\phi}(\phi_0)$ (green dashed line), $V_{b,\phi}(\phi_0)$ (red line), and $1.5V_{b,\phi}(\phi_0)$ (blue dashed line), respectively. The CMB pivot scale k_* corresponds to $\phi_*/m_P = 2.90$.

The plateau in $V_b(\phi)$ caused by $\delta V(\phi)$ leads inflation to the USR stage, during which the inflaton field alters extremely slowly, so the parameters ε and η change significantly. First, η becomes positive, with the value maintaining around $\mathcal{O}(1)$. Hence, we can define the starting and ending points of the USR stage by $\eta(N_s) = \eta(N_e) = 0$, with N_s and N_e being the corresponding numbers of e -folds. Second, ε decreases exponentially and induces a remarkable increase of the power spectrum $\mathcal{P}_{\mathcal{R}}(k)$. Altogether, the SR conditions are both broken in the USR stage, and the evolutions of ε and η are shown in Fig. 2.

Furthermore, the influences of $\delta V(\phi)$ on the power spectra $\mathcal{P}_{\mathcal{R}}(k)$ are shown in Fig. 3, where we plot the power spectra both by numerically solving Eq. (2.3) and from the SR approximations in Eq. (2.5). In addition, the nearly scale-invariant power spectrum is also shown for comparison.¹ The SR power spectrum significantly deviates from the numerical

¹Here, we should emphasize that it is the scales that exit the horizon before the USR stage that account for the sharp rise in $\mathcal{P}_{\mathcal{R}}(k)$. This is because, in the SR stage, $\mathcal{R}_{k,N}$ decreases exponentially outside the horizon, so \mathcal{R}_k is almost constant; in contrast, in the USR stage, $\mathcal{R}_{k,N}$ still increases outside the horizon, so \mathcal{R}_k can continue increasing. Consequently, there is a competition between the decrease and increase of $\mathcal{R}_{k,N}$, and they balance at a characteristic scale \tilde{k} [47]. Therefore, for the scales with $\tilde{k} < k < k(N_s)$ (i.e., the scales exiting the horizon before the USR stage but still in the SR stage), the increase of $\mathcal{R}_{k,N}$ in the USR stage can exceed the decrease of $\mathcal{R}_{k,N}$ in the SR stage, leading to the sharp rise in $\mathcal{P}_{\mathcal{R}}(k)$. This also explains the offset of the steep growth of $\mathcal{P}_{\mathcal{R}}(k)$ between the numerical result and the SR approximations [i.e., the numerical $\mathcal{P}_{\mathcal{R}}(k)$ rises up at smaller k].

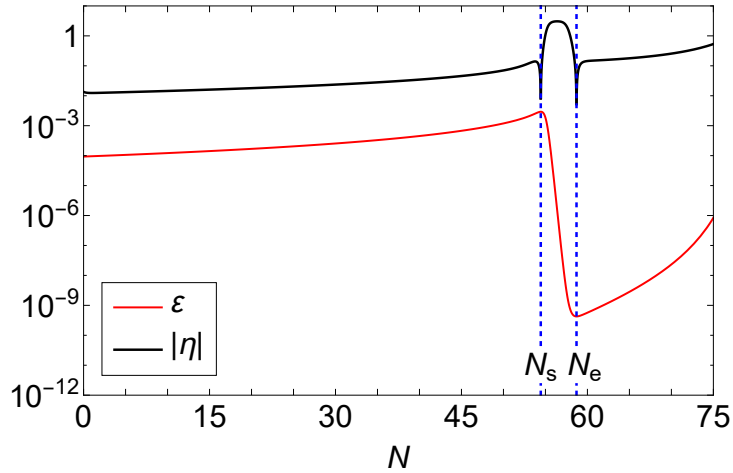


Figure 2. The parameters ε and η in the SR and USR stages, with the same model parameters as those in Fig. 1. The starting and ending points of the USR stage are defined by $\eta(N_s) = \eta(N_e) = 0$, with $N_s = 54.45$ and $N_e = 58.70$. During the USR stage, η is negative and maintains around $\mathcal{O}(1)$; ε decreases exponentially and leads to a remarkable increase of the power spectrum $\mathcal{P}_{\mathcal{R}}(k)$, to be shown in Fig. 3.

result, for both the position and height of its peak. Meanwhile, the PBH abundance is highly sensitive to these two factors, so the SR approximations cannot be trusted any longer in the USR stage, and all relevant calculations below are performed numerically.

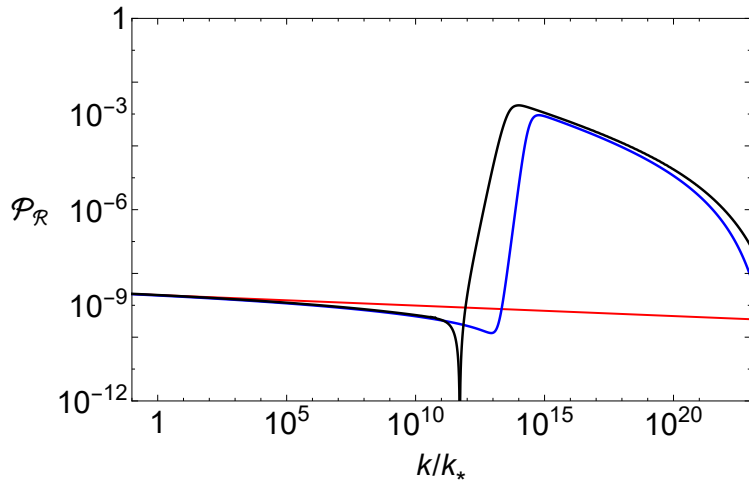


Figure 3. The power spectra $\mathcal{P}_{\mathcal{R}}(k)$ influenced by the perturbation $\delta V(\phi)$ in Eq. (4.3): the power spectrum by numerically solving Eq. (2.3) (black line), the power spectrum from the SR approximations in Eq. (2.5) (blue line), and the nearly scale-invariant power spectrum for comparison (red line), with the same model parameters as those in Fig. 1. The SR power spectrum significantly deviates from the numerical result, for both the position and height of its peak, and can no longer be trusted in the USR inflation.

Now, we calculate the power spectra $\mathcal{P}_{\mathcal{R}}(k)$ and demand the PBH abundances $f(M) \sim 0.1$, with the PBH masses M in the three typical mass windows at $10^{-17}M_{\odot}$, $10^{-13}M_{\odot}$, and $30M_{\odot}$, respectively. In this process, we have three model parameters A , ϕ_0 , and σ but only two constraints from M and f , so we will be confronted with the parameter degeneracy. Therefore, in this section, we further impose a restriction as $A = V_{\text{b},\phi}(\phi_0)$ for convenience, meaning that the perturbation $\delta V(\phi)$ can create a perfect plateau at ϕ_0 . Thus, our task is reduced to determining the remaining two parameters ϕ_0 and σ . Moreover, the parameter degeneracy can simultaneously result in slightly different scalar spectral index n_s and tensor-to-scalar r , and the bounds $n_s = 0.965 \pm 0.008$ and $r < 0.06$ (95% confidence level) [13] must be taken into account in parameter adjustment.

The power spectra $\mathcal{P}_{\mathcal{R}}(k)$ and the relevant PBH abundances $f(M)$ are plotted in Fig. 4, and the corresponding parameters ϕ_0 and σ are summarized in Tab. 1. We set the initial conditions for inflation to be $\phi/m_{\text{P}} = 3.30$ and $\phi_N/m_{\text{P}} = -0.0137$, and we have $n_s = 0.9591$ and $r = 0.00321$ ($10^{-17}M_{\odot}$), $n_s = 0.9588$ and $r = 0.00322$ ($10^{-13}M_{\odot}$), and $n_s = 0.9580$ and $r = 0.00322$ ($30M_{\odot}$), all in their 95% confidence levels [13].

M/M_{\odot}	ϕ_0/m_{P}	σ/m_{P}
10^{-17}	1.31	0.0831881
10^{-13}	1.81	0.0405471
30	2.56	0.0159387

Table 1. The parameters ϕ_0 and σ for the PBH abundances $f \sim 0.1$ in the three typical mass windows at $10^{-17}M_{\odot}$, $10^{-13}M_{\odot}$, and $30M_{\odot}$, respectively. With M increasing, ϕ_0 increases (the USR stage occurs earlier) and σ decreases (the duration of the USR stage shortens). Moreover, f is highly sensitive to σ .

From Fig. 4 and Tab. 1, our basic results can be summarized as follows. First, if the PBH abundances f are around 0.1, the power spectra $\mathcal{P}_{\mathcal{R}}$ should be enhanced up to at least 10^{-2} on small scales, seven orders of magnitude higher than the value on large scales (e.g., $\mathcal{P}_{\mathcal{R}} \sim 10^{-9}$ on the CMB pivot scale k_*). Second, with the PBH mass M increasing, the peak of $\mathcal{P}_{\mathcal{R}}$ moves to larger scales, as can be seen from Eq. (2.6) that a larger M corresponds to a smaller k_{PBH} . Moreover, a smaller k_{PBH} means an earlier USR stage, so the parameter ϕ_0 increases with M , as shown in Tab. 1. Third, a larger ϕ_0 would enhance $\mathcal{P}_{\mathcal{R}}$, so if the height of $\mathcal{P}_{\mathcal{R}}$ maintains around 10^{-2} , the parameter σ must decrease accordingly. This is because the earlier the USR inflation occurs (with larger ϕ_0), the more slowly the inflaton rolls down. Therefore, the width σ of the plateau must become smaller (with shorter duration of the USR stage), so that the influence of $\delta V(\phi)$ would not be too large, as also shown in Tab. 1. Last, the precision of σ is notably high, with at least six significant digits. This is expected, as from Eqs. (2.7) and (3.4), the PBH abundance $f(M)$ is exponentially sensitive to σ , so the step size of σ must be as small as $10^{-7}m_{\text{P}}$ in parameter adjustment.

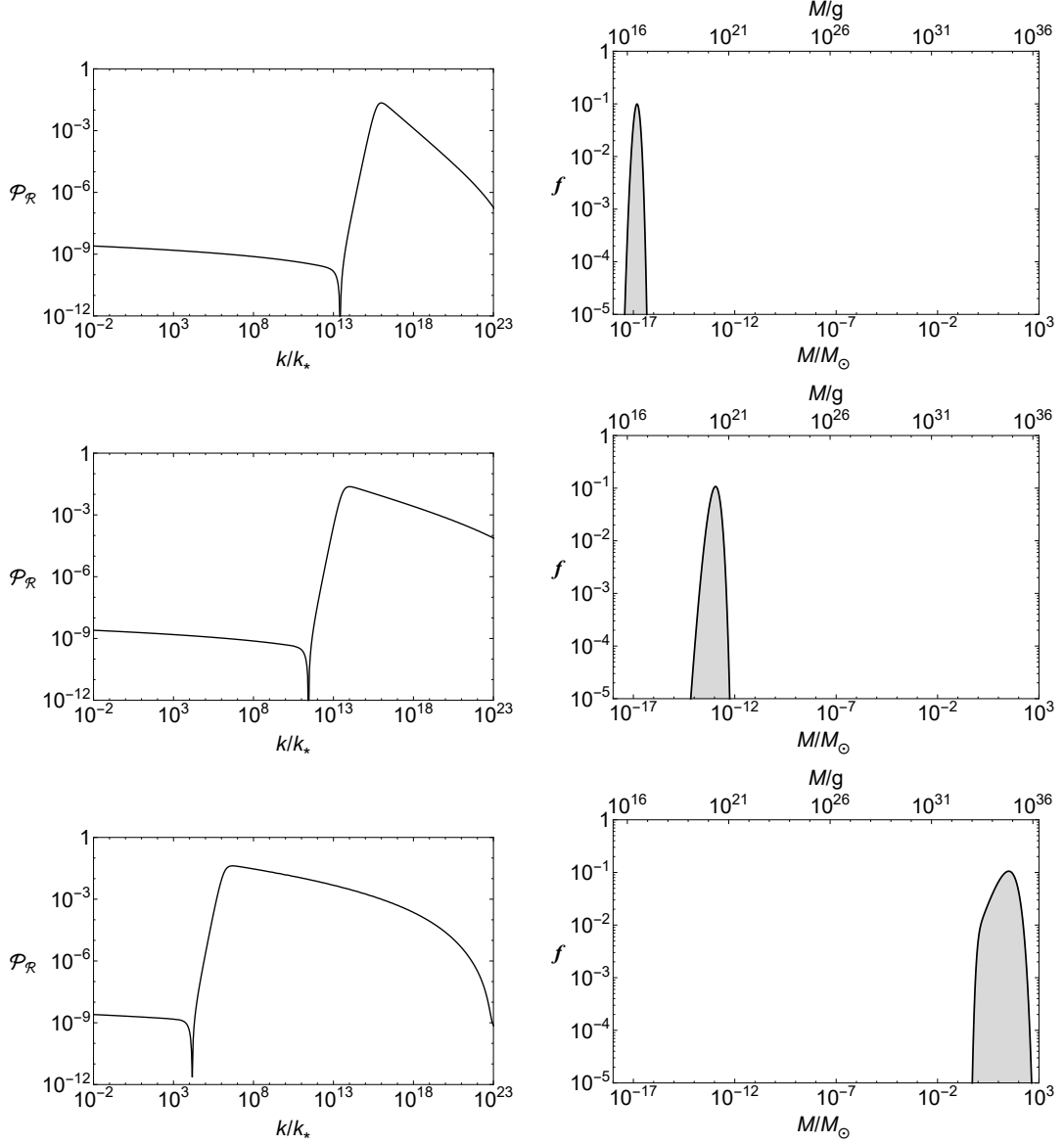


Figure 4. The power spectra $\mathcal{P}_{\mathcal{R}}(k)$ and the relevant PBH abundances $f(M)$ with the PBH masses M in the three typical mass windows at $10^{-17}M_{\odot}$, $10^{-13}M_{\odot}$, and $30M_{\odot}$, respectively. If $f \sim 0.1$, $\mathcal{P}_{\mathcal{R}}$ needs to be enhanced up to at least 10^{-2} on small scales, seven orders of magnitude higher than its value on large scales. From Eq. (2.6), with M increasing, k_{PBH} decreases, so the peak of $\mathcal{P}_{\mathcal{R}}(k)$ moves to larger scales.

5 PBHs from two perturbations in the inflaton potential

In this section, we further investigate the cases with two perturbations in the inflaton potential in the GLMS approximation, in which there can be PBHs of different masses both with the abundance $f \sim 0.1$ in two of the three typical mass windows at $10^{-17}M_{\odot}$, $10^{-13}M_{\odot}$, and $30M_{\odot}$.

Below, the F function in Eq. (4.1) is chosen to be Gaussian,

$$\delta V(\phi) = -A(\phi - \phi_0) \exp \left[-\frac{(\phi - \phi_0)^2}{2\sigma^2} \right], \quad (5.1)$$

and the reasons are twofold. One is to verify the applicability of our model by simply taking the perturbation in another form; the other and more essential one is to avoid the interference between the two perturbations. First, the two perturbations cannot be too far away; otherwise, the inflaton will spend more time on the first plateau on large scale and will pass the second plateau on small scale much later, making the relevant PBH mass extremely small. Second, the two perturbations cannot be too close either; otherwise, there will be strong parameter degeneracy. Consequently, the two perturbations should be separated at a moderate distance, and at the same time the two plateaus should be narrower than before. Compared to the Lorentzian form in Eq. (4.3), the Gaussian form in Eq. (5.1) converges more quickly and can avoid the interference more effectively. Now, the inflaton potential reads $V(\phi) = V_b(\phi) + \delta V_1(\phi) + \delta V_2(\phi)$.

In the current case with two perturbations, it is impossible to set $A = V_{b,\phi}(\phi_0)$ for each perturbation any longer. Therefore, we re-parameterize A in the form of $A = V_{b,\phi}(\phi_0)(1 + A_0)$, with A_0 characterizing the deviation of the inflaton potential from a perfect plateau at ϕ_0 . Altogether, there are six model parameters: $A_0^{(1)}$, $\phi_0^{(1)}$, $\sigma^{(1)}$, $A_0^{(2)}$, $\phi_0^{(2)}$, and $\sigma^{(2)}$ (the superscripts 1 and 2 stand for small and large PBH masses, respectively).

According to the separation between the two PBH masses, the power spectra $\mathcal{P}_{\mathcal{R}}(k)$ and the relevant PBH abundances $f(M)$ are plotted in Fig. 5, and the corresponding model parameters are summarized in Tab. 2. The initial conditions for inflation are kept the same as those in Sec. 4, and the changes of the resulting n_s and r are negligible.

M/M_\odot	$A_0^{(1)}$	$\phi_0^{(1)}/m_{\text{P}}$	$\sigma^{(1)}/m_{\text{P}}$	$A_0^{(2)}$	$\phi_0^{(2)}/m_{\text{P}}$	$\sigma^{(2)}/m_{\text{P}}$	$(\phi_0^{(2)} - \phi_0^{(1)})/m_{\text{P}}$
10^{-17} and 10^{-13}	0.2736210	1.700	0.029705	0.1383814	1.810	0.029002	0.110
10^{-13} and 30	0.0121025	2.377	0.0200459	0.0160910	2.521	0.0164554	0.144
10^{-17} and 30	0.0119941	2.165	0.0260763	0.0180321	2.522	0.0162205	0.357

Table 2. The parameters $A_0^{(1)}$, $\phi_0^{(1)}$, $\sigma^{(1)}$, $A_0^{(2)}$, $\phi_0^{(2)}$, and $\sigma^{(2)}$ (the superscripts 1 and 2 stand for small and large PBH masses, respectively) for the PBHs of different masses both with the abundance $f \sim 0.1$ in two of the three typical mass windows at $10^{-17}M_\odot$, $10^{-13}M_\odot$, and $30M_\odot$. With the separation between the two mass windows decreasing, the separation between the two perturbations $\Delta\phi = \phi_0^{(2)} - \phi_0^{(1)}$ also decreases, but A_0 increases, so as to avoid the interference between the two USR stages.

From Fig. 5 and Tab. 2, we arrive at the following results. First, analogous to the case with one perturbation, if the PBH abundances f are around 0.1 in two mass windows simultaneously, the power spectra $\mathcal{P}_{\mathcal{R}}(k)$ must also possess two peaks both with the height of 10^{-2} . Second, from the first and last columns in Tab. 2, we observe that the separation between the two perturbations $\Delta\phi = \phi_0^{(2)} - \phi_0^{(1)}$ increases with that between the two mass windows, and this tendency also applies to the separation between the two peaks in $\mathcal{P}_{\mathcal{R}}(k)$. Third, as $\Delta\phi$ decreases, the parameter A_0 increases. This is because, when the two

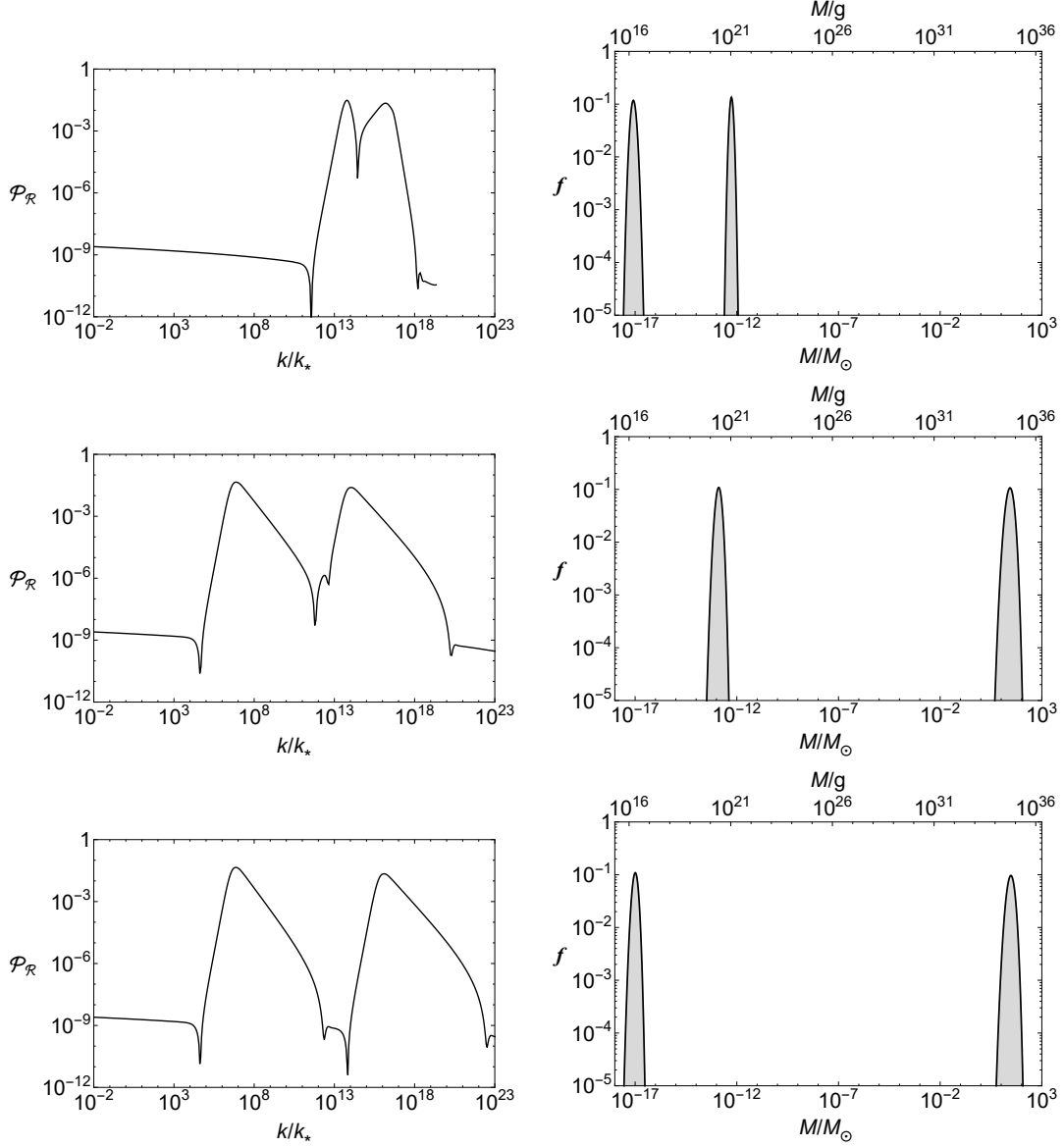


Figure 5. The power spectra $\mathcal{P}_{\mathcal{R}}(k)$ and the relevant PBH abundances $f(M)$ with the PBHs of different masses in two of the three typical mass windows at $10^{-17}M_{\odot}$, $10^{-13}M_{\odot}$, and $30M_{\odot}$. The interference between the two perturbations in the inflaton potential induces a turning point in the growing stage of $\mathcal{P}_{\mathcal{R}}(k)$ on the small scale (middle left panel). This turning point tends to disappear when the two perturbations are far away (lower left panel) and also disappears when the two perturbations are too close, but with a strong distortion in $\mathcal{P}_{\mathcal{R}}(k)$ at the same time (upper left panel).

perturbations are closer, we must be very cautious to avoid their interference. However, this cannot be done simply by decreasing the width σ of the perturbation, because if σ is too small, the USR stage cannot last long enough to enhance $\mathcal{P}_{\mathcal{R}}(k)$ to 10^{-2} as needed. Therefore, a larger A_0 is indispensable, so as to incline the plateau and to play a similar role of a smaller σ . Fourth, we point out an interesting feature in $\mathcal{P}_{\mathcal{R}}(k)$ in Fig. 5: the turning

point in the growing stage of $\mathcal{P}_{\mathcal{R}}(k)$ on the small scale. This is a natural consequence of the interference between the two perturbations, which induces an overlap between the decaying stage of $\mathcal{P}_{\mathcal{R}}(k)$ on the large scale and the growing stage of $\mathcal{P}_{\mathcal{R}}(k)$ on the small scale. This turning point can be clearly seen, if the two perturbations are separated at a moderate distance (middle left panel). Moreover, if the two perturbations are far away, the turning point tends to disappear (lower left panel); if they are too close, the turning point also disappears, but there is a strong distortion in $\mathcal{P}_{\mathcal{R}}(k)$ (upper left panel).

6 Comparison of peak and PS theories

The PBH abundance f depends not only on the power spectrum, but also on the specific methods to calculate the PBH mass fraction β . In Sec. 3, we have discussed three different approximations based on the general peak theory, according to the spectral moments involved. In Secs. 4 and 5, we use only the GLMS approximation. Now, we compare all these three approximations in calculating the PBH abundance, with one perturbation in the inflaton potential.

First, we compare the PBH abundances obtained from the high-peak and GLMS approximations, with the PBH mass being around $10^{-13}M_{\odot}$. As explained in Sec. 3, the PBH mass fraction β_{hp} is only slightly less than β_{GLMS} (too little to be distinguished, especially in the logarithmic coordinate system in Fig. 4), and the difference mainly stems from the γ factor. In Fig. 6, the PBH abundance obtained from the GLMS approximation is set to be 0.1, with the relevant factors being $\nu_c = 8.82676$ and $\gamma = 0.823356$. Therefore, from Eqs. (3.3) and (3.4),

$$\frac{\beta_{\text{hp}}}{\beta_{\text{GLMS}}} = \frac{\nu_c^2 + 2 - 3/\gamma^2}{\nu_c^2 - 1} = 0.981428.$$

The slight difference lies in the fact that ν_c is much greater than 1, as the PBH formation is a rather rare event. This ratio indicates that the discrepancy between the high-peak and GLMS approximations is almost negligible in calculating the PBH abundance, and setting $\gamma \approx 1$ in the GLMS approximation (i.e., considering only the zeroth and first spectral moments) is reasonable and safe. This conclusion is also valid for the PBH mass windows at $10^{-17}M_{\odot}$ and $30M_{\odot}$.

Furthermore, we compare the PBH abundances obtained from the GLMS approximation and the PS theory, with the PBH masses in the three typical mass windows. In Fig. 7, the PBH abundances obtained from the GLMS approximation are set to be 0.1, and we observe that the PBH abundances obtained from the PS theory are merely $10^{-4} \sim 10^{-3}$, two or three orders of magnitude lower, indicating that the PS theory significantly underestimates the PBH abundance. This can be understood from Eq. (3.6). At the leading order of ν_c , we have

$$\frac{\beta_{\text{PS}}}{\beta_{\text{GLMS}}} \approx \frac{1}{(Q\nu_c)^3},$$

with $\nu_c \gg 1$ taken into account. The numerical results of $\beta_{\text{PS}}/\beta_{\text{GLMS}}$ and the specific values of ν_c , Q , and $1/(Q\nu_c)^3$ are summarized in Tab. 3, and we find that the theoretical values of $1/(Q\nu_c)^3$ agree with the numerical ratios of $\beta_{\text{PS}}/\beta_{\text{GLMS}}$ very well.

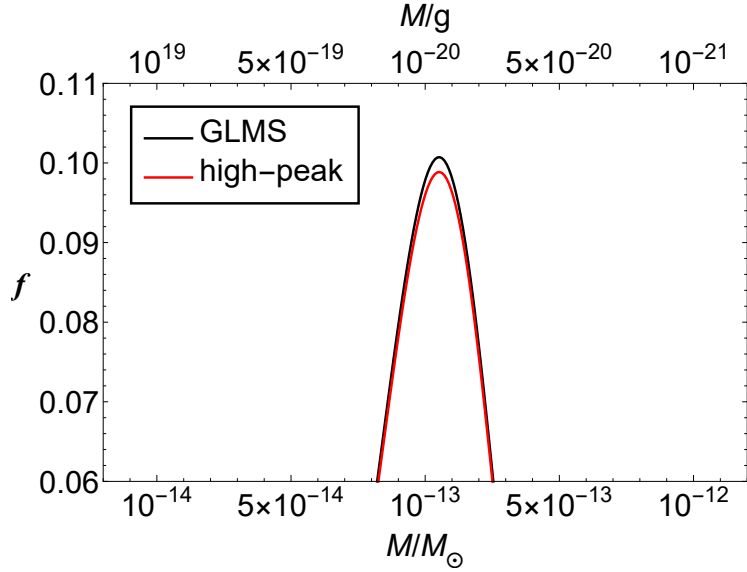


Figure 6. The PBH abundances $f(M)$ obtained from the GLMS approximation (black line) and the high-peak approximation (red line), with the PBH mass being around $10^{-13}M_{\odot}$. The $f(M)$ from the GLMS approximation is set to be 0.1, and the $f(M)$ from the high-peak approximation is 0.981428. This slight difference is from the facts that $\nu_c = 8.82676 \gg 1$ and $\gamma = 0.823356 \approx 1$, so the ratio of $\beta_{\text{hp}}/\beta_{\text{GLMS}}$ is pretty close to 1, consistent with Eqs. (3.3) and (3.4).

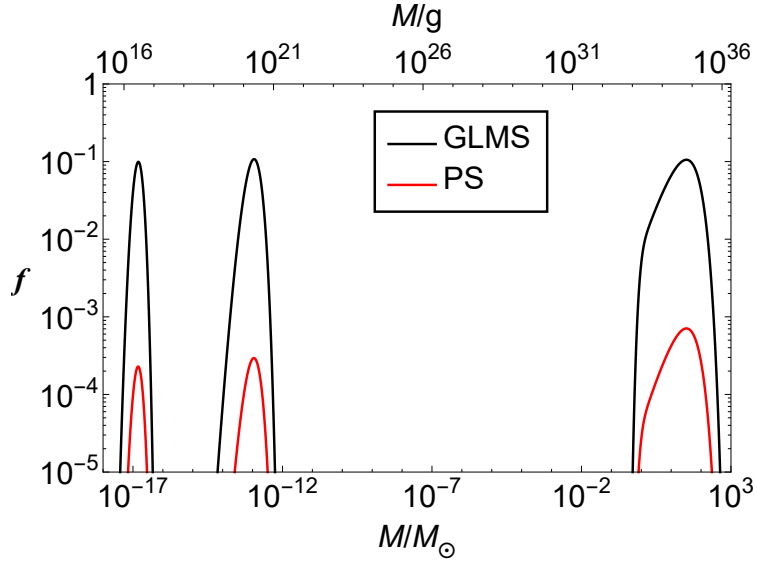


Figure 7. The PBH abundances $f(M)$ obtained from the GLMS approximation (black lines) and the PS theory (red lines), with the PBH masses in the three typical mass windows at $10^{-17}M_{\odot}$, $10^{-12}M_{\odot}$, and $30M_{\odot}$, respectively. The $f(M)$ from the GLMS approximation are set to be 0.1, and the $f(M)$ from the PS theory are only 2.30547×10^{-4} , 2.73895×10^{-4} , and 6.71296×10^{-4} , respectively, two or three orders of magnitude lower. Therefore, the PS theory systematically underestimates the PBH abundance than peak theory.

M/M_\odot	$\beta_{\text{PS}}/\beta_{\text{GLMS}}$	ν_c	Q	$1/(Q\nu_c)^3$
10^{-17}	0.00230547	9.33184	0.814301	0.00227899
10^{-13}	0.00273195	8.82676	0.813913	0.00269689
30	0.00671296	6.57976	0.811961	0.00655791

Table 3. The numerical ratios of the PBH mass fraction $\beta_{\text{PS}}/\beta_{\text{GLMS}}$ obtained from the GLMS approximation and the PS theory and the theoretical values of $1/(Q\nu_c)^3$ at the leading order of ν_c . As $\nu_c \sim \mathcal{O}(10) \gg 1$, the theoretical results agree with the numerical ratios very well.

Altogether, the PS theory has a systematic bias from the high-peak and GLMS approximations. Hence, the agreements of the PBH abundances obtained in Refs. [71, 72] apply only to the power spectra in the power-law form or with a running spectral index, but are no longer valid for the power spectrum with a peak on small scales due to the USR inflation. Moreover, it was also pointed out that the underestimation of the PBH abundance from the PS theory will be further enlarged, if the extended mass function is taken into account [77].

7 Conclusion

The research on PBHs is an interesting combination of black hole physics and cosmology, greatly promoted by the discovery of the merging GWs from binary black holes in recent years. One of the fundamental motivations to study PBHs is to seek an effective candidate for DM. Currently, compared with the WIMP-like or axion-like DM candidates, the experimental constraints on PBHs are still rather loose. Therefore, the aim of our work is to phenomenologically study the PBH abundance by considering the perturbations in the inflaton potential. We systematically calculate the power spectrum $\mathcal{P}_{\mathcal{R}}$ and the PBH abundance f via the GLMS approximation of peak theory, with the high-peak approximation and the PS theory also carefully investigated for comparison. Our basic conclusions can be drawn as follows.

(1) The perturbations in the inflaton potential can significantly decelerate the local velocity of the inflaton, driving inflation into the USR stage, during which the usual SR approximations are invalidated, and the primordial curvature perturbation \mathcal{R} still increases outside the horizon. By this means, the power spectrum $\mathcal{P}_{\mathcal{R}}$ is remarkably enhanced on small scales, producing the PBHs with desirable masses and abundances.

(2) The specific form of the perturbation is constructed to be antisymmetric in the USR region, with three model parameters A , ϕ_0 , and σ , so that the perturbation can be smoothly imposed on the background inflaton potential on both sides of the USR region. Thus, a perfect plateau can be created, and the USR stage can be maintained for a sufficiently long time. In this way, the adjustments of model parameters become much easier, and the fine-tuning problem frequently encountered in the USR inflation can be greatly relieved.

(3) In the case of one perturbation, we can achieve the PBHs with $f \sim 0.1$ in the three typical mass windows at $10^{-17}M_\odot$, $10^{-13}M_\odot$, and $30M_\odot$, respectively. With M increasing,

ϕ_0 increases, as the large-mass PBH exits the horizon earlier. At the same time, σ decreases, as the inflaton rolls down more slowly in the early era, so the duration of the USR stage must be shortened; otherwise, $\mathcal{P}_{\mathcal{R}}$ would be too high.

(4) In the case of two perturbations, we can also achieve the PBHs of different masses both with $f \sim 0.1$ in two of the three typical mass windows. The distance between the two perturbations increases with that between the two mass windows, and the plateaus become more inclined when the two perturbations are close, in order to avoid their interference to a greater extent. Moreover, due to this interference, there is a turning point in the growing stage of $\mathcal{P}_{\mathcal{R}}$ on the small scale.

(5) The PBH abundances obtained from the high-peak and GLMS approximations are almost the same, because we always have $\nu_c \gg 1$ and $\gamma \approx 1$. However, the PBH abundance obtained from the PS theory is two or three orders of magnitude lower. This underestimation is mainly due to the fact that the PS theory is based on a non-physical dimensional reduction of the general peak theory, so there is systematic bias between it and the high-peak or GLMS approximation, especially in the USR inflation. In general, peak theory is based on a sounder theoretical footing, and the PS theory should be regarded as its limit case, so the relevant results must be treated with great caution.

Last, we should mention that the PBH abundance is also affected by many other ingredients, among which the most influential is the threshold of density contrast δ_c (or ν_c). From Eqs. (3.3)–(3.5), we observe that the PBH mass fraction is exponentially sensitive to ν_c . The specific value of the threshold for the PBH formation is a long-debated issue in the literature [81–91] and is affected by a number of aspects, such as the profile of density contrast, the equation of state of the cosmic medium, and the primordial non-Gaussianity. Therefore, in this paper, we follow the most frequently used value $\delta_c = 0.414$ [85]. This is also the reason that we have not compared the PBH abundance with all currently available experimental constraints, because the focus of this work is not the elaborate adjustments of model parameters that can be equivalently replaced by a small change of the threshold, but is the antisymmetric construction of the perturbation in the inflaton potential and the comparison of peak and PS theories in calculating the PBH abundance.

Acknowledgments

We are very grateful to Zhao-Hui Chen, Florian Kühnel, Jing Liu, Dominik Schwarz, and Ji-Xiang Zhao for fruitful discussions. This work is supported by the Fundamental Research Funds for the Central Universities of China (No. N182410001).

References

- [1] B. P. Abbott *et al.* (LIGO Scientific and Virgo Collaboration), *Observation of gravitational waves from a binary black hole merger*, *Phys. Rev. Lett.* **116** (2016) 061102, [arXiv:1602.03837\[gr-qc\]](#).
- [2] M. Sasaki, T. Suyama, T. Tanaka, and S. Yokoyama, *Primordial black holes—perspectives in gravitational wave astronomy*, *Class. Quant. Grav.* **35** (2018) 063001, [arXiv:1801.05235\[astro-ph\]](#).

- [3] B. Carr, K. Kohri, Y. Sendouda, and J. Yokoyama, *Constraints on primordial black holes*, [arXiv:2002.12778\[astro-ph\]](https://arxiv.org/abs/2002.12778).
- [4] M. Yu. Khlopov, *Primordial black holes*, *Res. Astron. Astrophys.* **10** (2010) 495, [arXiv:0801.0116\[astro-ph\]](https://arxiv.org/abs/0801.0116).
- [5] A. M. Green and B. J. Kavanagh, *Primordial black holes as a dark matter candidate*, *J. Phys. G* **48** (2021) 043001, [arXiv:2007.10722\[astro-ph\]](https://arxiv.org/abs/2007.10722).
- [6] K. M. Belotsky *et al.*, *Signatures of primordial black hole dark matter*, *Mod. Phys. Lett. A* **29** (2014) 1440005, [arXiv:1410.0203\[astro-ph\]](https://arxiv.org/abs/1410.0203).
- [7] B. Carr and F. Kühnel, *Primordial black holes as dark matter: recent developments*, *Ann. Rev. Nucl. Part. Sci.* **70** (2020) 355, [arXiv:2006.02838\[astro-ph\]](https://arxiv.org/abs/2006.02838).
- [8] Ya. B. Zel'dovich and I. D. Novikov, *The hypothesis of cores retarded during expansion and the hot cosmological model*, *Sov. Astron. AJ (Engl. Transl.)* **10** (1967) 602.
- [9] S. W. Hawking, *Gravitationally collapsed objects of very low mass*, *Mon. Not. Roy. Astron. Soc.* **152** (1971) 75.
- [10] B. J. Carr and S. W. Hawking, *Black holes in the early Universe*, *Mon. Not. Roy. Astron. Soc.* **168** (1974) 399.
- [11] B. J. Carr, *The primordial black hole mass spectrum*, *Astrophys. J.* **201** (1975) 1.
- [12] <https://github.com/bradkav/PBHbounds>.
- [13] N. Aghanim *et al.* (Planck Collaboration), *Planck 2018 results. VI. Cosmological parameters*, *Astron. Astrophys.* **641** (2020) A6, [arXiv:1807.06209\[astro-ph\]](https://arxiv.org/abs/1807.06209).
- [14] P. Ivanov, P. Naselsky, and I. Novikov, *Inflation and primordial black holes as dark matter*, *Phys. Rev. D* **50** (1994) 7173.
- [15] J. García-Bellido, A. D. Linde, and D. Wands, *Density perturbations and black hole formation in hybrid inflation*, *Phys. Rev. D* **54** (1996) 6040, [arXiv:9605094\[astro-ph\]](https://arxiv.org/abs/9605094).
- [16] S. M. Leach, M. Sasaki, D. Wands, and A. R. Liddle, *Enhancement of superhorizon scale inflationary curvature perturbations*, *Phys. Rev. D* **64** (2001) 023512, [arXiv:0101406\[astro-ph\]](https://arxiv.org/abs/0101406).
- [17] W. H. Kinney, *Horizon crossing and inflation with large eta*, *Phys. Rev. D* **72** (2005) 023515, [arXiv:0503017\[gr-qc\]](https://arxiv.org/abs/0503017).
- [18] S. Chongchitnan and G. Efstathiou, *Accuracy of slow-roll formulae for inflationary perturbations: implications for primordial black hole formation*, *J. Cosmol. Astropart. Phys.* **01** (2007) 011, [arXiv:0611818\[astro-ph\]](https://arxiv.org/abs/0611818).
- [19] J. Martin, H. Motohashi, and T. Suyama, *Ultra slow-roll inflation and the non-Gaussianity consistency relation*, *Phys. Rev. D* **87** (2013) 023514, [arXiv:1211.0083\[astro-ph\]](https://arxiv.org/abs/1211.0083).
- [20] S. Clesse and J. García-Bellido, *Massive primordial black holes from hybrid inflation as dark matter and the seeds of galaxies*, *Phys. Rev. D* **92** (2015) 023524, [arXiv:1501.07565\[astro-ph\]](https://arxiv.org/abs/1501.07565).
- [21] J. García-Bellido and E. R. Morales, *Primordial black holes from single field models of inflation*, *Phys. Dark Univ.* **18** (2017) 47, [arXiv:1702.03901\[astro-ph\]](https://arxiv.org/abs/1702.03901).
- [22] K. Kannike, L. Marzola, M. Raidal, and H. Veermäe, *Single field double inflation and*

- primordial black holes, *J. Cosmol. Astropart. Phys.* **09** (2017) 020, [arXiv:1705.06225\[astro-ph\]](#).
- [23] C. Germani and T. Prokopec, *On primordial black holes from an inflection point*, *Phys. Dark Univ.* **18** (2017) 6, [arXiv:1706.04226\[astro-ph\]](#).
- [24] H. Motohashi and W. Hu, *Primordial black holes and slow-roll violation*, *Phys. Rev. D* **96** (2017) 063503, [arXiv:1706.06784\[astro-ph\]](#).
- [25] K. Dimopoulos, *Ultra slow-roll inflation demystified*, *Phys. Lett. B* **775** (2017) 262, [arXiv:1707.05644\[hep-ph\]](#).
- [26] J. M. Ezquiaga, J. García-Bellido, and E. R. Morales, *Primordial black hole production in critical higgs inflation*, *Phys. Lett. B* **776** (2018) 345, [arXiv:1705.04861\[astro-ph\]](#).
- [27] G. Ballesteros and M. Taoso, *Primordial black hole dark matter from single field inflation*, *Phys. Rev. D* **97** (2018) 023501, [arXiv:1709.05565\[hep-ph\]](#).
- [28] M. Cicoli, V. A. Diaz, and F. G. Pedro, *Primordial black holes from string inflation*, *J. Cosmol. Astropart. Phys.* **06** (2018) 034, [arXiv:1803.02837\[hep-th\]](#).
- [29] O. Özsoy, S. Parameswaran, G. Tasinato, and I. Zavala, *Mechanisms for primordial black hole production in string theory*, *J. Cosmol. Astropart. Phys.* **07** (2018) 005, [arXiv:1803.07626\[hep-th\]](#).
- [30] H. Di and Y. Gong, *Primordial black holes and second order gravitational waves from ultra-slow-roll inflation*, *J. Cosmol. Astropart. Phys.* **07** (2018) 007, [arXiv:1707.09578\[astro-ph\]](#).
- [31] M. Biagetti, G. Franciolini, A. Kehagias, and A. Riotto, *Primordial black holes from inflation and quantum diffusion*, *J. Cosmol. Astropart. Phys.* **07** (2018) 032, [arXiv:1804.07124\[astro-ph\]](#).
- [32] T.-J. Gao and Z.-K. Guo, *Primordial black hole production in inflationary models of supergravity with a single chiral superfield*, *Phys. Rev. D* **98** (2018) 063526, [arXiv:1806.09320\[hep-ph\]](#).
- [33] C. Germani and I. Musco, *Abundance of primordial black holes depends on the shape of the inflationary power spectrum*, *Phys. Rev. Lett.* **122** (2019) 141302, [arXiv:1805.04087\[astro-ph\]](#).
- [34] I. Dalianis, A. Kehagias, and G. Tringas, *Primordial black holes from α -attractors*, *J. Cosmol. Astropart. Phys.* **01** (2019) 037, [arXiv:1805.09483\[astro-ph\]](#).
- [35] D. Cruces, C. Germani, and T. Prokopec, *Failure of the stochastic approach to inflation beyond slow-roll*, *J. Cosmol. Astropart. Phys.* **03** (2019) 048, [arXiv:1807.09057\[gr-qc\]](#).
- [36] S. Passaglia, W. Hu, and H. Motohashi, *Primordial black holes and local non-Gaussianity in canonical inflation*, *Phys. Rev. D* **99** (2019) 043536, [arXiv:1812.08243\[astro-ph\]](#).
- [37] G. Ballesteros, J. B. Jiménez, and M. Pieroni, *Black hole formation from a general quadratic action for inflationary primordial fluctuations*, *J. Cosmol. Astropart. Phys.* **06** (2019) 016, [arXiv:1811.03065\[astro-ph\]](#).
- [38] S.-L. Cheng, W. Lee, and K.-W. Ng, *Superhorizon curvature perturbation in ultraslow-roll inflation*, *Phys. Rev. D* **99** (2019) 063524, [arXiv:1811.10108\[astro-ph\]](#).
- [39] C. T. Byrnes, P. S. Cole, and S. P. Patil, *Steepest growth of the power spectrum and*

- primordial black holes, *J. Cosmol. Astropart. Phys.* **06** (2019) 028, [arXiv:1811.11158\[astro-ph\]](#).
- [40] S. A. Vallejo-Peña and A. E. Romano, *Are primordial black holes produced by entropy perturbations in single field inflationary models?*, *J. Cosmol. Astropart. Phys.* **11** (2019) 015, [arXiv:1904.07503\[astro-ph\]](#).
- [41] C. Pattison, V. Vennin, H. Assadullahi, and D. Wands, *Stochastic inflation beyond slow roll*, *J. Cosmol. Astropart. Phys.* **07** (2019) 031, [arXiv:1905.06300\[astro-ph\]](#).
- [42] C. Fu, P. Wu, and H. Yu, *Primordial black holes from inflation with nonminimal derivative coupling*, *Phys. Rev. D* **100** (2019) 063532, [arXiv:1907.05042\[astro-ph\]](#).
- [43] P. Carrilho, K. A. Malik, and D. J. Mulryne, *Dissecting the growth of the power spectrum for primordial black holes*, *Phys. Rev. D* **100** (2019) 103529, [arXiv:1907.05237\[astro-ph\]](#).
- [44] N. Bhaumik and R. K. Jain, *Primordial black holes dark matter from inflection point models of inflation and the effects of reheating*, *J. Cosmol. Astropart. Phys.* **01** (2020) 037, [arXiv:1907.04125\[astro-ph\]](#).
- [45] H. Motohashi, S. Mukohyama, and M. Oliosi, *Constant roll and primordial black holes*, *J. Cosmol. Astropart. Phys.* **03** (2020) 002, [arXiv:1910.13235\[gr-qc\]](#).
- [46] R. Mahbub, *Primordial black hole formation in inflationary α -attractor models*, *Phys. Rev. D* **101** (2020) 023533, [arXiv:1910.10602\[astro-ph\]](#).
- [47] J. Liu, Z.-K. Guo, and R.-G. Cai, *Analytical approximation of the scalar spectrum in the ultraslow-roll inflationary models*, *Phys. Rev. D* **101** (2020) 083535, [arXiv:2003.02075\[astro-ph\]](#).
- [48] J. Lin, Q. Gao, Y. Gong, Y. Lu, C. Zhang, and F. Zhang, *Primordial black holes and secondary gravitational waves from k and G inflation*, *Phys. Rev. D* **101** (2020) 103515, [arXiv:2001.05909\[gr-qc\]](#).
- [49] S. S. Mishra and V. Sahni, *Primordial black holes from a tiny bump/dip in the inflaton potential*, *J. Cosmol. Astropart. Phys.* **04** (2020) 007, [arXiv:1911.00057\[gr-qc\]](#).
- [50] R.-G. Cai, Z.-K. Guo, J. Liu, L. Liu, and X.-Y. Yang, *Primordial black holes and gravitational waves from parametric amplification of curvature perturbations*, *J. Cosmol. Astropart. Phys.* **06** (2020) 013, [arXiv:1912.10437\[astro-ph\]](#).
- [51] G. Ballesteros, J. Rey, M. Taoso, and A. Urbano, *Stochastic inflationary dynamics beyond slow-roll and consequences for primordial black hole formation*, *J. Cosmol. Astropart. Phys.* **08** (2020) 043, [arXiv:2006.14597\[astro-ph\]](#).
- [52] K. Kefala, G. P. Kodaxis, I. D. Stamou, and N. Tetradis, *Features of the inflaton potential and the power spectrum of cosmological perturbations*, *Phys. Rev. D* **104** (2021) 023506, [arXiv:2010.12483\[astro-ph\]](#).
- [53] D. G. Figueroa, S. Raatikainen, S. Räsänen, and E. Tomberg, *Non-Gaussian tail of the curvature perturbation in stochastic ultraslow-roll inflation: implications for primordial black hole production*, *Phys. Rev. Lett.* **127** (2021) 101302, [arXiv:2012.06551\[astro-ph\]](#).
- [54] O. Özsoy and Z. Lalak, *Primordial black holes as dark matter and gravitational waves from bumpy axion inflation*, *J. Cosmol. Astropart. Phys.* **01** (2021) 040, [arXiv:2008.07549\[astro-ph\]](#).

- [55] G. Tasinato, *An analytic approach to non-slow-roll inflation*, *Phys. Rev. D* **103** (2021) 023535, [arXiv:2012.02518\[hep-th\]](#).
- [56] H. V. Ragavendra, P. Saha, L. Sriramkumar, and J. Silk, *PBHs and secondary GWs from ultraslow roll and punctuated inflation*, *Phys. Rev. D* **103** (2021) 083510, [arXiv:2008.12202\[astro-ph\]](#).
- [57] C. Pattison, V. Vennin, D. Wands, and H. Assadullahi, *Ultra-slow-roll inflation with quantum diffusion*, *J. Cosmol. Astropart. Phys.* **04** (2021) 080, [arXiv:2101.05741\[astro-ph\]](#).
- [58] K.-Y. Choi, S.-b. Kang, and R. N. Raveendran, *Reconstruction of potentials of hybrid inflation in the light of primordial black hole formation*, *J. Cosmol. Astropart. Phys.* **06** (2021) 054, [arXiv:2102.02461\[astro-ph\]](#).
- [59] M. Solbi and K. Karami, *Primordial black holes and induced gravitational waves in Galileon inflation*, *J. Cosmol. Astropart. Phys.* **08** (2021) 056, [arXiv:2102.05651\[astro-ph\]](#).
- [60] K. Inomata, E. McDonough, and W. Hu, *Primordial black holes arise when the inflaton falls*, [arXiv:2104.03972\[astro-ph\]](#).
- [61] S. Kawai and J. Kim, *CMB from a Gauss-Bonnet-induced de Sitter fixed point*, *Phys. Rev. D* **104** (2021) 043525, [arXiv:2105.04386\[hep-ph\]](#).
- [62] R. Zheng, J. Shi, and T. Qiu, *On primordial black holes generated from inflation with solo/multi-bumpy potential*, [arXiv:2106.04303\[astro-ph\]](#).
- [63] F. Zhang, J. Lin, and Y. Lu, *A double-peaked inflation model: scalar induced gravitational waves and PBH suppression from primordial non-Gaussianity*, *Phys. Rev. D* **104** (2021) 063515, [arXiv:2106.10792\[gr-qc\]](#).
- [64] L.-H. Liu and W.-L. Xu, *The primordial black hole from running curvature*, [arXiv:2107.07310\[astro-ph\]](#).
- [65] S. Heydari and K. Karami, *Primordial black holes in nonminimal derivative coupling inflation driven by quartic potential*, [arXiv:2107.10550\[gr-qc\]](#).
- [66] S. Kawai and J. Kim, *Primordial black holes from Gauss-Bonnet-corrected single field inflation*, *Phys. Rev. D* **104** (2021) 083545, [arXiv:2108.01340\[astro-ph\]](#).
- [67] D. Artigas, J. Grain, and V. Vennin, *Hamiltonian formalism for cosmological perturbations: the separate-universe approach*, [arXiv:2110.11720\[astro-ph\]](#).
- [68] S. Heydari and K. Karami, *Primordial black holes ensued from exponential potential and coupling parameter in nonminimal derivative inflation model*, [arXiv:2111.00494\[gr-qc\]](#).
- [69] A. G. Doroshkevich, *Spatial structure of perturbations and origin of galactic rotation in fluctuation theory*, *Astrophysics* **6** (1970) 320.
- [70] J. M. Bardeen, J. R. Bond, N. Kaiser, and A. S. Szalay, *The statistics of peaks of Gaussian random fields*, *Astrophys. J.* **304** (1986) 15.
- [71] A. M. Green, A. R. Liddle, K. A. Malik, and M. Sasaki, *A new calculation of the mass fraction of primordial black holes*, *Phys. Rev. D* **70** (2004) 041502(R), [arXiv:0403181\[astro-ph\]](#).
- [72] S. Young, C. T. Byrnes, and M. Sasaki, *Calculating the mass fraction of primordial black holes*, *J. Cosmol. Astropart. Phys.* **07** (2014) 045, [arXiv:1405.7023\[gr-qc\]](#).

- [73] C. M. Yoo, T. Harada, J. Garriga, and K. Kohri, *Primordial black hole abundance from random Gaussian curvature perturbations and a local density threshold*, *Prog. Theor. Exp. Phys.* **2018** (2018) 123E01, [arXiv:1805.03946\[astro-ph\]](#).
- [74] C. M. Yoo, J. O. Gong, and S. Yokoyama, *Abundance of primordial black holes with local non-Gaussianity in peak theory*, *J. Cosmol. Astropart. Phys.* **09** (2019) 033, [arXiv:1906.06790\[astro-ph\]](#).
- [75] C. Germani and R. K. Sheth, *Nonlinear statistics of primordial black holes from Gaussian curvature perturbations*, *Phys. Rev. D* **101** (2020) 063520, [arXiv:1912.07072\[astro-ph\]](#).
- [76] S. Young and M. Musso, *Application of peaks theory to the abundance of primordial black holes*, *J. Cosmol. Astropart. Phys.* **11** (2020) 022, [arXiv:2001.06469\[astro-ph\]](#).
- [77] Y.-P. Wu, *Peak statistics for the primordial black hole abundance*, *Phys. Dark Univ.* **30** (2020) 100654, [arXiv:2005.00441\[astro-ph\]](#).
- [78] C. M. Yoo, T. Harada, S. Hirano, and K. Kohri, *Abundance of primordial black holes in peak theory for an arbitrary power spectrum*, *Prog. Theor. Exp. Phys.* **2021** (2021) 013E02, [arXiv:2008.02425\[astro-ph\]](#).
- [79] R. Mahbub, *Primordial black hole formation in α -attractor models: an analysis using optimized peaks theory*, *Phys. Rev. D* **104** (2021) 043506, [arXiv:2103.15957\[astro-ph\]](#).
- [80] W. H. Press and P. Schechter, *Formation of galaxies and clusters of galaxies by self-similar gravitational condensation*, *Astrophys. J.* **187** (1974) 425.
- [81] J. C. Niemeyer and K. Jedamzik, *Dynamics of primordial black hole formation*, *Phys. Rev. D* **59** (1999) 124013, [arXiv:9901292\[astro-ph\]](#).
- [82] I. Musco, J. C. Miller, and L. Rezzolla, *Computations of primordial black hole formation*, *Class. Quant. Grav.* **22** (2005) 1405, [arXiv:0412063\[gr-qc\]](#).
- [83] I. Musco, J. C. Miller, and A. G. Polnarev, *Primordial black hole formation in the radiative era: Investigation of the critical nature of the collapse*, *Class. Quant. Grav.* **26** (2009) 235001, [arXiv:0811.1452\[gr-qc\]](#).
- [84] I. Musco and J. C. Miller, *Primordial black hole formation in the early universe: critical behaviour and self-similarity*, *Class. Quant. Grav.* **30** (2013) 145009, [arXiv:1201.2379\[gr-qc\]](#).
- [85] T. Harada, C. M. Yoo, and K. Kohri, *Threshold of primordial black hole formation*, *Phys. Rev. D* **88** (2013) 084051, [arXiv:1309.4201\[astro-ph\]](#).
- [86] T. Nakama, T. Harada, A. G. Polnarev, and J. Yokoyama, *Identifying the most crucial parameters of the initial curvature profile for primordial black hole formation*, *J. Cosmol. Astropart. Phys.* **01** (2014) 037, [arXiv:1310.3007\[gr-qc\]](#).
- [87] I. Musco, *Threshold for primordial black holes: Dependence on the shape of the cosmological perturbations*, *Phys. Rev. D* **100** (2019) 123524, [arXiv:1809.02127\[gr-qc\]](#).
- [88] A. Escrivà, *Simulation of primordial black hole formation using pseudo-spectral methods*, *Phys. Dark Univ.* **27** (2020) 100466, [arXiv:1907.13065\[gr-qc\]](#).
- [89] A. Escrivà, C. Germani, and R. K. Sheth, *Universal threshold for primordial black hole formation*, *Phys. Rev. D* **101** (2020) 044022, [arXiv:1907.13311\[gr-qc\]](#).
- [90] A. Escrivà, C. Germani, and R. K. Sheth, *Analytical thresholds for black hole formation in*

general cosmological backgrounds, *J. Cosmol. Astropart. Phys.* **01** (2021) 030,
[arXiv:2007.05564\[gr-qc\]](#).

- [91] I. Musco, V. De Luca, G. Franciolini, and A. Riotto, *Threshold for primordial black holes. II. A simple analytic prescription*, *Phys. Rev. D* **103** (2021) 063538,
[arXiv:2011.03014\[astro-ph\]](#).
- [92] S. Kachru, R. Kallosh, A. D. Linde, and S. P. Trivedi, *De Sitter vacua in string theory*, *Phys. Rev. D* **68** (2003) 046005, [arXiv:0301240\[hep-th\]](#).